

Article

The Different Effects of Two Types of El Niño on Eastern China's Spring Precipitation During the Decaying Stages

Dezhi Zhang ^{1,2}, Chujie Gao ^{1,2,*} , Zhichao Yang ^{1,2} , Zhi Yuan ^{1,2}, Xuanke Wang ^{1,2}, Bei Xu ^{2,3} and Haozhong Qian ⁴

¹ Key Laboratory of Marine Hazards Forecasting, Ministry of Natural Resources, Hohai University, Nanjing 210098, China; 2113010122@hhu.edu.cn (Z.Y.); 2113010329@hhu.edu.cn (Z.Y.); 2113010123@hhu.edu.cn (X.W.)

² College of Oceanography, Hohai University, Nanjing 210098, China; xubei@jit.edu.cn

³ College of Intelligent Science and Control Engineering, Jinling Institute of Technology, Nanjing 211169, China

⁴ Wuxi Meteorological Bureau of Jiangsu Province, Wuxi 214135, China; wuxiqhz@163.com

* Correspondence: gaochujie@foxmail.com or gaochujie@hhu.edu.cn

Abstract: El Niño is one of the most significant global climatic phenomena affecting the East Asian atmospheric circulation and climate. This study uses multi-source datasets, including observations and analyses, and statistical methods to investigate the variations and potential causes of boreal spring precipitation anomalies in eastern China under different El Niño sea surface temperature conditions, namely, the Eastern Pacific and Central Pacific (EP and CP) El Niño cases. The findings reveal that, particularly along the Yangtze–Huaihe valley, spring precipitation markedly increases in most regions of eastern China during the EP El Niño decaying stages. Conversely, during the CP El Niño decaying stages, precipitation anomalies are weak, with occurrences of weak negative anomalies in the same regions. Further analyses reveal that during the decaying spring of different El Niño cases, differences in the location and strength of the Northwest Pacific (NWP) abnormal anticyclone, which is associated with the central–eastern Pacific warm sea surface temperature anomaly (SSTA), result in distinct anomalous precipitation responses in eastern China. The SSTA center of the EP El Niño is more easterly and stronger. In the meantime, NWP abnormal anticyclones are more easterly and have a broader range, facilitating water vapor transport over eastern China. By contrast, the CP El Niño SSTA center is westward and relatively weaker, leading to a relatively weak, westward, and narrower anomalous NWP anticyclone that causes less significant water vapor transport anomalies in eastern China. This paper highlights the diverse impacts of El Niño diversity on regional atmospheric circulation and precipitation, providing valuable scientific references for studying regional climate change in East Asia.

Keywords: El Niño; eastern China; precipitation; anticyclone; southern China; regional climate



Citation: Zhang, D.; Gao, C.; Yang, Z.; Yuan, Z.; Wang, X.; Xu, B.; Qian, H. The Different Effects of Two Types of El Niño on Eastern China's Spring Precipitation During the Decaying Stages. *Atmosphere* **2024**, *15*, 1331. <https://doi.org/10.3390/atmos15111331>

Academic Editors: Lei Liu and Dachao Jin

Received: 18 September 2024

Revised: 1 November 2024

Accepted: 3 November 2024

Published: 5 November 2024



Copyright: © 2024 by the authors. Licensee MDPI, Basel, Switzerland. This article is an open access article distributed under the terms and conditions of the Creative Commons Attribution (CC BY) license (<https://creativecommons.org/licenses/by/4.0/>).

1. Introduction

El Niño is a dominant interannual climate variability pattern that critically affects global climate dynamics, particularly influencing atmospheric circulation in East Asia. It impacts the East Asian circulation and climate at various stages in its lifecycle. During the development period of some El Niño cases, an anomalous cyclone dominates the Northwest Pacific (NWP) region, and the Western Pacific Subtropical High weakens, resulting in an anomalous northeasterly flow [1]. More importantly, as the decay period begins, an anomalous anticyclone prevails over the NWP, peaking in the winter and typically lasting until the summer [2]. Numerous studies have shown that El Niño's influence on the East Asia climate is evident, as it regulates the NWP abnormal anticyclone during its decaying period [3–6]. This anticyclone leads to significant anomalies in subtropical high pressure and water vapor transport, thereby exerting an influence on East Asian precipitation in the decaying year of an El Niño event [3,7].

Recent studies have identified an increase in occurrences of an atypical El Niño variant in the equatorial central Pacific, known as “El Niño Modoki” or the “Central Pacific El Niño” (CP El Niño), which exhibits distinct sea surface temperature anomaly (SSTA) patterns compared to the traditional Eastern Pacific El Niño (EP El Niño) [8–11]. The CP El Niño case displays notable variations in its spatial features and formation mechanisms compared to the EP El Niño case [12,13]. Theories such as the Delayed Oscillator Theory and the Indo-Western Pacific Ocean Capacitor, which apply to the EP El Niño case, do not apply to the CP El Niño case [10,14]. While the EP El Niño case has a larger spatial scale regarding the SSTA and atmospheric response, the signals of the SSTA persist in the mid-Pacific across the developing and decaying phases of the CP El Niño cases [15]. These findings indicate significant differences in the SSTA patterns and circulation responses between the CP and EP El Niño cases.

For eastern China, spring precipitation accounts for about 30% of the annual precipitation in south China (SC) and also plays an important role in the annual precipitation of the Yangtze–Huaihe valley. Its significance in Chinese agriculture cannot be overstated, as it provides essential moisture for crops and aids in temperature recovery. Unfortunately, extreme spring weather has become increasingly common in recent years, particularly in SC and the Yangtze–Huaihe valley, where heavy precipitation events have frequently occurred. These weather patterns are often linked to El Niño [16], presenting significant risks to transportation, production activities, and travel safety. Thus, understanding the differential impacts of various El Niño cases on precipitation is essential for agricultural planning, economic development, and disaster mitigation in eastern China.

Due to the significant differences between the two types of El Niño SSTA patterns and the local circulation responses [9–11], the corresponding precipitation characteristics are markedly different. For example, the spring anomalous precipitation modes of the EP El Niño exhibit a positive–negative–positive (+/–/+) mode from East Asia to the equatorial Pacific. In contrast, the CP El Niño shows the opposite (–/+/–) anomalous precipitation mode (Figure 1). This variation corresponds directly with their respective SSTAs and atmospheric responses [1]. Specifically, during the decaying stage of the EP El Niño, the negative SSTA in the NWP suppresses local convection, promoting a Rossby wave-induced anomalous anticyclone. Concurrently, the warm SSTA in the equatorial eastern Pacific strengthens the NWP abnormal anticyclone (NWPAAC) through the Walker circulation, which substantially reduces precipitation in the NWP [2,3]. On the other hand, the CP El Niño features weaker air–sea interactions and less pronounced impacts on the NWPAAC and regional precipitation anomalies due to the weak SSTA [17].

The anticyclones induced by El Niño in the NWP exhibit distinct characteristics, leading to divergent atmospheric circulation and precipitation patterns in East Asia. Notably, the precipitation anomalies in eastern China during the spring of both types of El Niño exhibit a strong asymmetry, which is tightly linked to the NWPAAC [18]. Spring is a period of dramatic changes in the East Asian atmospheric circulation, and weather systems such as Siberian high pressure and South Asian high pressure interact with El Niño [19,20], bringing a variety of changes in spring precipitation and also bringing more difficulties in sub-seasonal to seasonal forecasting. It is worth noting that the effect of the El Niño diversity on the NWPAAC pattern and, subsequently, the precipitation anomaly in eastern China during the decaying stage has not been fully discussed.

Numerous studies have examined the effects of the two types of El Niño phenomena on spring precipitation in East Asia [18,21,22]. Building on previous studies, this present study aims to further explore the impacts of the two types of El Niño on spring precipitation in eastern China. It focuses on comparing the effects of the EP El Niño and CP El Niño on spring precipitation in this region and analyzing the relevant physical mechanisms and differences between them. Section 2 introduces the datasets and methods used in this study. Section 3 summarizes the two types of El Niño-related anomalies in spring, especially the precipitation anomalies in SC and the Yangtze–Huaihe valley. Section 4 discusses the underlying physical mechanisms between the spring precipitation anomalies and the two

types of El Niño phenomena in East Asia. Finally, the conclusions and discussions are given in Section 5.

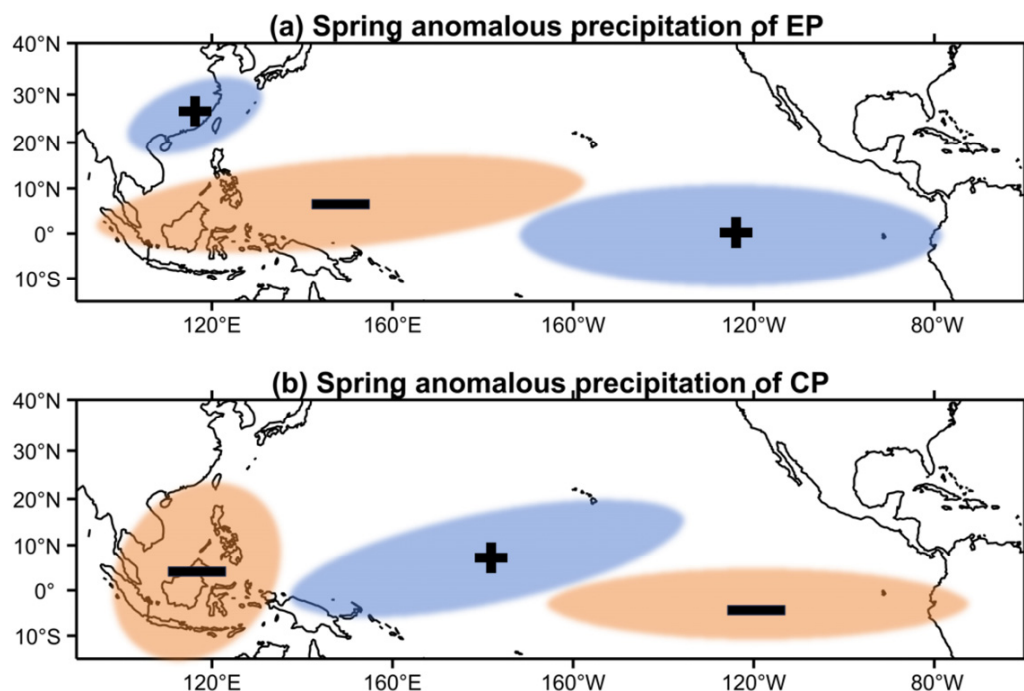


Figure 1. Schematic diagram of spring precipitation anomalies in the (a) EP El Niño and (b) CP El Niño cases. The colored area indicates a significant precipitation anomaly and the +/− indicates a positive/negative precipitation anomaly. The diagram is drawn based on the results of Yuan and Yang [1].

2. Data and Methods

The monthly SST dataset from 1870 to the present has a 1° × 1° resolution derived from the Hadley Centre Sea Ice and SST dataset [23]. The Japan 55-year reanalysis dataset, produced by the Japan Meteorological Agency, has a horizontal resolution of 1.25° × 1.25° and spans 1958–2020 [24], providing monthly atmospheric fields, such as three-dimensional wind speed and humidity. The precipitation data were obtained from the U.K. National Centre for Atmospheric Sciences (NCAS) CRU TS climate dataset [25] with a resolution of 0.5° × 0.5°, covering the period of 1901–2020. In addition, this study uses the National Oceanic and Atmospheric Administration (NOAA) Monthly SST index (ERSSTv5). The study period is 1961–2020, which is expected for all datasets, and all the data were detrended before making the calculations, which removed the effects of climate change.

In this study, the events with five consecutive months with the Niño 3.4 (170° W–120° W, 5° S–5° N) SSTA index greater than 0.5 were selected and defined as El Niño cases, and 21 El Niño cases were selected for the 1961–2020 period (Table 1). Regarding the classification of the two types of El Niño events, we used the Niño cold tongue/Niño warm pool (NCT/NWP) indices [26] to classify El Niño cases, which are defined as follows:

$$\begin{cases} \text{NCT} = \text{Nio 3} - \alpha \text{Nio 4} \\ \text{NWP} = \text{Nio 4} - \alpha \text{Nio 3} \end{cases} \begin{cases} \alpha = 0.4, \text{Nio 3} * \text{Nio 4} > 0 \\ \alpha = 0.0, \text{Otherwise} \end{cases}$$

where the Niño 3 (5° N–5° S, 150°–90° W) and Niño 4 (5° N–5° S, 160° E–150° W) indices are calculated by averaging the winter (December–February, DJF) SSTAs. These indices have been widely employed to study the El Niño diversity and its climatic effects [27–31].

Table 1. The selected El Niño events for the 1960–2020 period.

TYPE	YEAR
EP	1963/64, 1965/66, 1969/70, 1972/73, 1976/77, 1982/83, 1986/87, 1991/92, 1997/98, 2002/03, 2006/07, 2009/10, 2015/16
CP	1968/69, 1977/78, 1979/80, 1987/88, 1994/95, 2004/05, 2014/15, 2018/19

The main patterns of the two El Niño types, i.e., different El Niño phase propagation and El Niño state changes, can be easily characterized using these two indices [31]. Here, we simultaneously compared the magnitude of the winter NCT/NWP indices (Figure 2) for the selected years, and the year was categorized as the EP(CP) El Niño when the NCT (NWP) index was more extensive. The selection of the years was based on the NCT/NWP indices, and, in some of them, the two indices were more similar, e.g., 1987/1988, 2002/2003, 2006/2007, and 2009/2010 (Figure 2). If these years were to be excluded, the final results would still support our view. MAM (March–April) in this paper represents the spring.

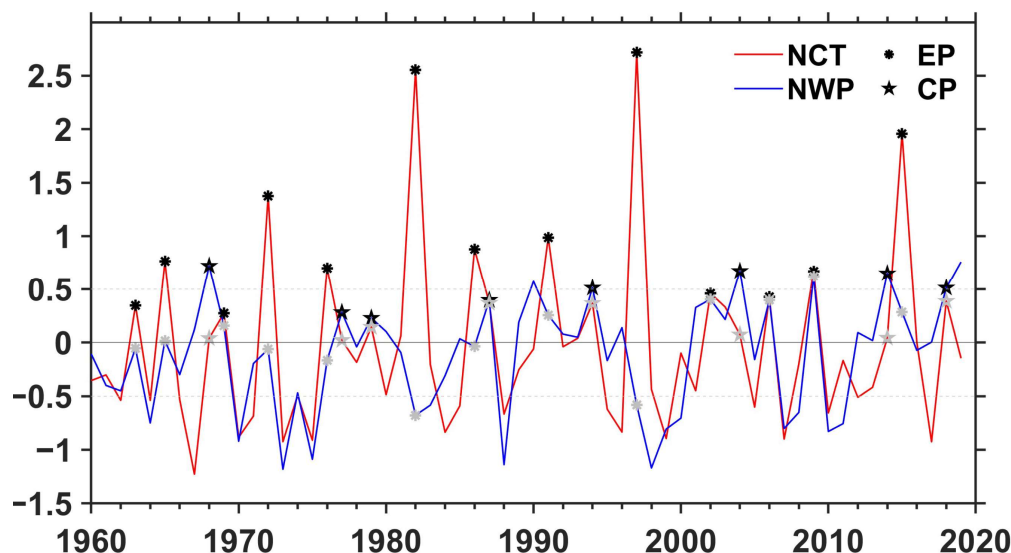


Figure 2. NCT (DJF) and NWP (DJF) indices (unit: °C) from 1960 to 2020.

3. Two Types of El Niño-Related SSTA and Precipitation Anomaly in Spring

3.1. SSTA Characteristics in Two El Niño Cases

A succinct overview of the SSTA characteristics associated with the two types of El Niño cases has been well documented by Jin et al. [10], Yu and Kao [14], and Yuan and Yang [1]. The El Niño phenomenon typically initiates in summer, intensifies during winter, and subsides in the subsequent year. During this cycle, the equatorial east–central Pacific experiences anomalous warming, while the NWP undergoes anomalous cooling. Simultaneously, the Indian Ocean begins to warm rapidly, which continues into the following summer. Figure 3 illustrates the distribution of the regression coefficients of the SSTA on the NCT/NWP indices from the El Niño developing period to the decaying period. The SSTA patterns of the two El Niño cases show marked differences: the EP El Niño SSTA center is stable in the equatorial eastern Pacific from its developing to decaying stages, while the CP El Niño SSTA center shows a westward shift and is stable in the mid-equatorial Pacific. Unlike the EP El Niño, which displays an extensive positive SSTA along the Peruvian coast, the CP El Niño variation exhibits no significant SSTA over there.

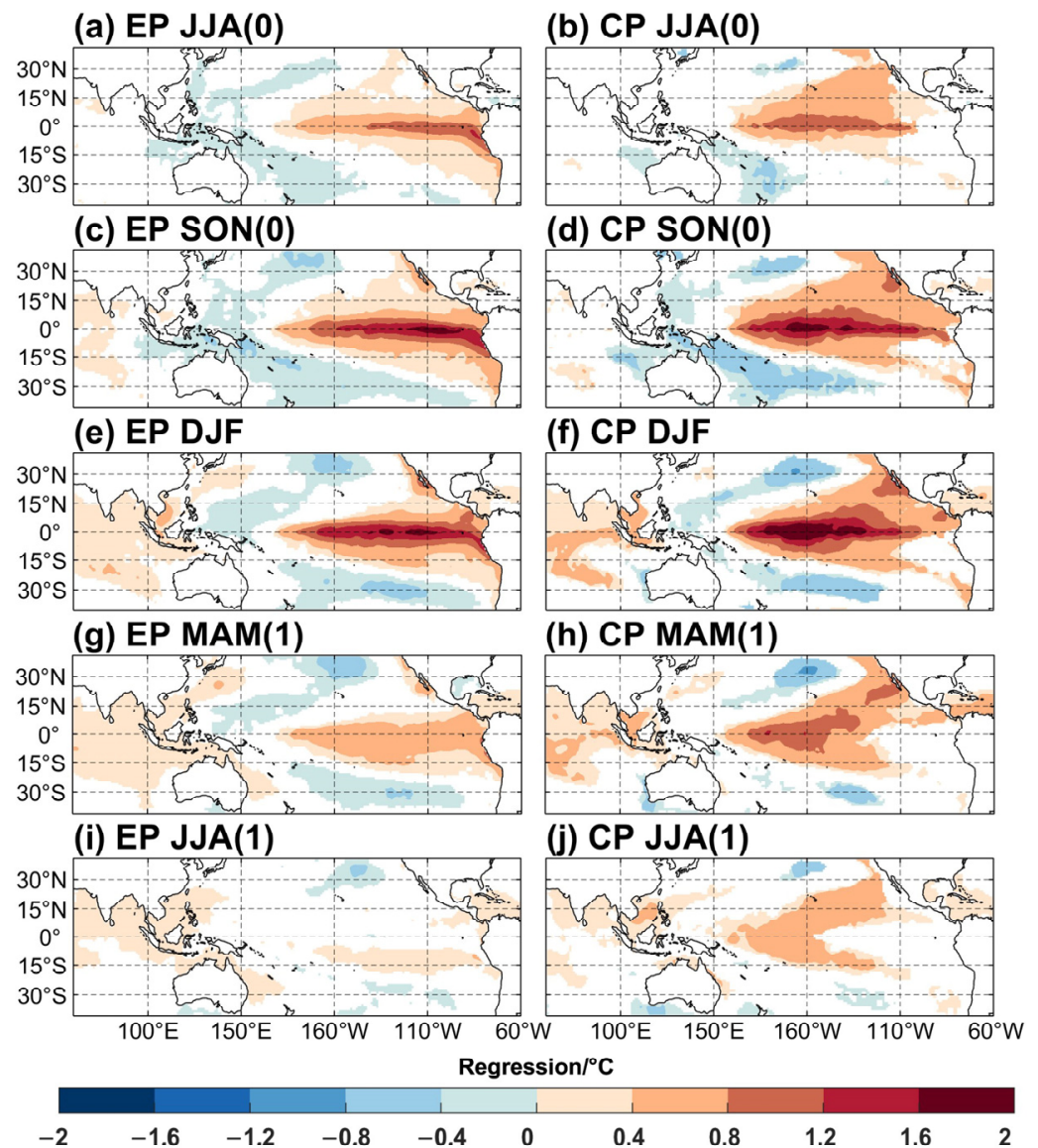


Figure 3. Regression of seasonal SSTA (unit: °C) on (left) NCT and (right) NWP for (a,b) previous summer, (c,d) previous autumn, (e,f) winter, (g,h) subsequent spring, and (i,j) subsequent summer. Colored areas indicate regression coefficients above the 95% confidence level.

For the spring SSTA, the positive SSTA signals of the EP El Niño are generally distributed east of the 180° meridian (Figure 3g), while those of the CP El Niño are near the 150° E (Figure 3h). The EP El Niño has significant cold SSTA signals in the western Pacific Ocean, while that in the CP El Niño barely passes the significance test. The warm SSTAs in the NWP of the CP El Niño are weaker than those of the EP El Niño and tend to be located more westward. In addition, the distribution and intensity of the SSTAs in the Indian Ocean also show great differences, with a stronger positive SSTA and more widely distributed SSTA in the EP El Niño cases and a weaker positive SSTA and smaller distributed SSTA in the CP El Niño cases. The warm SSTA in the equatorial central Pacific, the cold SSTA in the NWP, and the warm SSTA in the Indian Ocean are all significantly different, which together regulate and influence the local circulation in East Asia, especially the development and decline of the NWPAAC [31].

Both the intensity of the SSTA and the distribution of the SSTA modes are evidently different in the two types of El Niño cases. The SSTA in the mid-east Pacific Ocean can influence the East Asian climate through atmospheric circulation adjustments. Therefore, the

responses of the East Asian climate to the two El Niño cases are expected to be significantly different.

3.2. Different Precipitation Anomalies in Eastern China During El Niño Decaying Springs

El Niño mainly influences the East Asian circulation through the Pacific–East Asian teleconnection regulating the NWPAAC [2]. Specifically, this anticyclone has a direct impact on precipitation in eastern China by influencing the position of the subtropical high pressure and regulating the water vapor transport [3]. Earlier studies suggested that the occurrence of El Niño favored the transport of tropical warm moisture into SC and further north through the southwesterly winds to the northwest of the anomalous anticyclone, which created favorable conditions for widespread precipitation in SC and the Yangtze–Huaihe valley. However, recent studies have shown a significant difference between the impacts of the CP and EP El Niño on spring precipitation in SC [7,14,31,32].

To verify the different spring precipitation responses between the two types of El Niño cases, both correlation and composite analyses were utilized for showing the spring precipitation anomalies during the El Niño cases. The results are similar and robust (Figures 3 and 4). Specifically, positive precipitation anomalies occur in SC and the Yangtze–Huaihe valley, especially in the Yangtze–Huaihe valley for the EP El Niño. Meanwhile, significant anomalous precipitation conditions occurred further north (Figures 4a and 5a). In contrast, the same areas were covered by average or weak positive precipitation anomalies when the CP El Niño occurred (Figures 4b and 5b), and most areas failed the significance test. It should be noted that the correlation analysis in Figure 4 differs from the anomaly synthesis analysis in Figure 5, but the characteristics of the precipitation anomalies in the Yangtze–Huaihe valley, SC, and north China are similar. All in all, the above results indicate that there is a strong asymmetry in precipitation in SC during the decaying spring of the two types of El Niño [1,7,18,33]. The physical mechanisms behind the significant differences deserve further exploration.

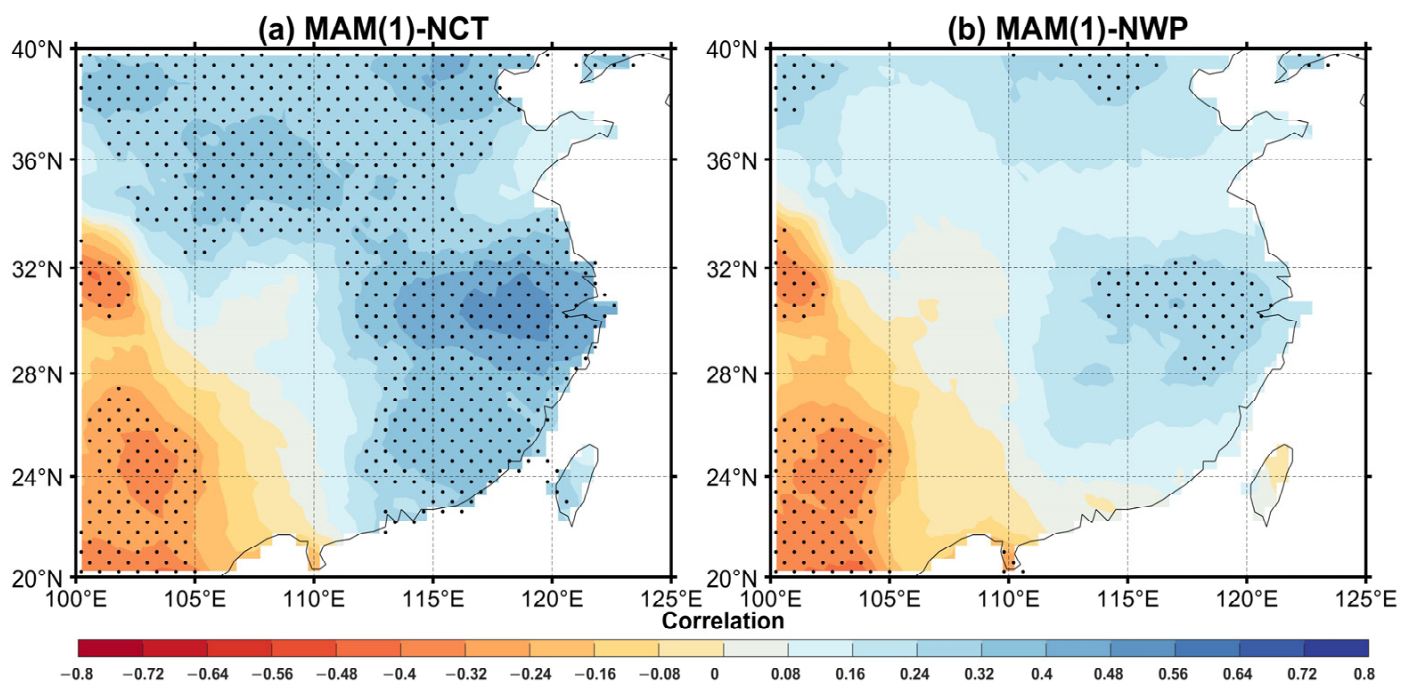


Figure 4. Correlations of MAM anomalous precipitation of the following year with (a) NCT and (b) NWP indices. The dotted areas indicate correlation coefficients above the 95% confidence level.

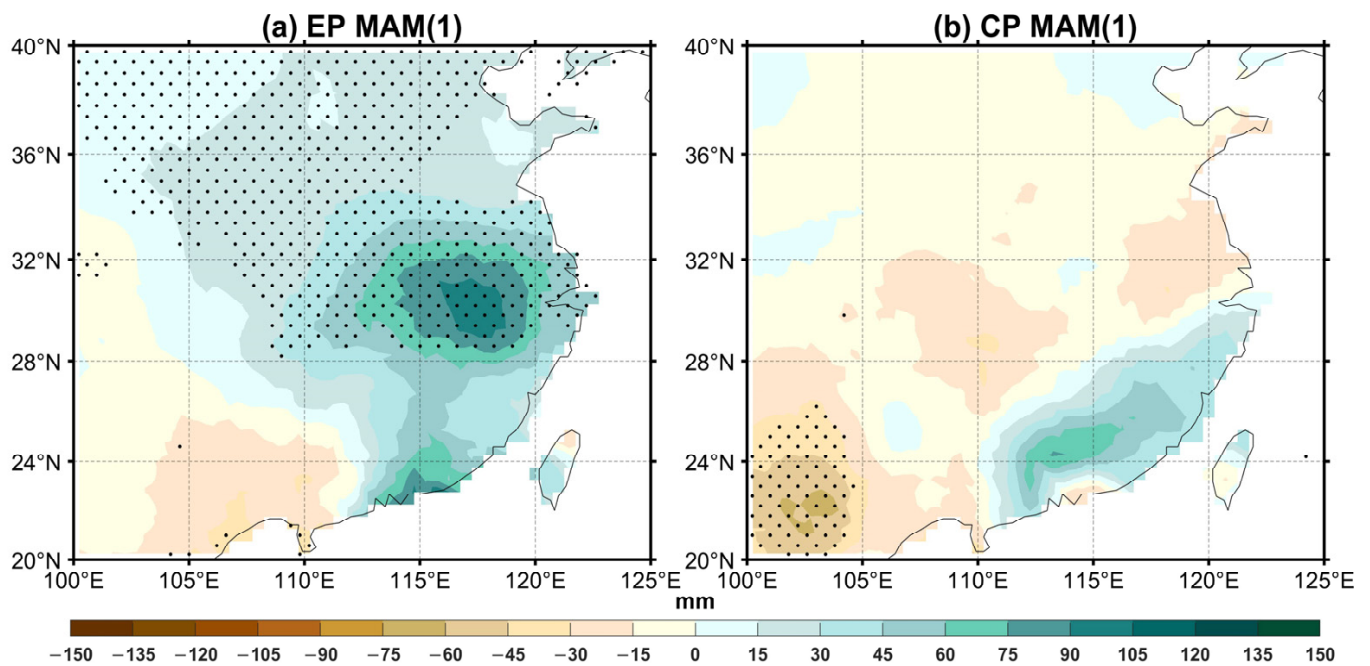


Figure 5. Composites of MAM anomalous cumulated precipitation (unit: mm) over East Asia in the (a) EP El Niño and (b) CP El Niño cases. The dotted areas indicate the composite anomalies above the 95% confidence level.

4. Physical Mechanisms in Eastern China's Spring Precipitation Responding to the Two Types of El Niño Cases

The two types of El Niño-related anomalies have been described previously, especially the precipitation differences in eastern China during the decaying spring. Therefore, the focus is on understanding how the EP El Niño and CP El Niño variants influence precipitation anomalies during the decaying spring, thereby unraveling the underlying physical mechanisms driving these variations.

Figure 6 illustrates the monthly evolution of the SSTA in the equatorial central–eastern Pacific from the developing to decaying stages for the two types of El Niño cases. From the summer of the developing period to the spring of the decaying period, the Niño 3 SSTA of the EP El Niño was significantly larger than that of the Niño 4 SSTA, and the central position of the SSTA was maintained in the east Pacific (Figure 6a). The intensity of the Niño 3 SSTA for the CP El Niño during the developing period was almost equal to that of the Niño 4 sea area (Figure 6b). However, the SSTA in the Niño 3 area declined rapidly from the winter to the decaying spring. In contrast, the SSTA in the Niño 4 area declined slowly in the CP El Niño. This led to a significantly larger Niño SSTA than Niño 4 from the DJF period onwards, which implies that the SSTA center was more westward during the CP El Niño decaying spring. It is worth mentioning that the intensity of the EP El Niño SSTA was generally greater than that of the CP El Niño from the winter to the decaying spring (Figure 6c). The two types of El Niño cases have significant differences in the SSTA central position and SSTA intensity. Therefore, this study suggests that both of the elements may play important roles in the East Asian circulation response.

Anomalous warming in the equatorial central–eastern Pacific from winter to the decaying spring of both the EP and CP El Niño causes a lower troposphere anomalous convergence. Concurrently, the equatorial Pacific experiences anomalous latitudinal winds (Figure 7). As El Niño transitions into its decaying phase, the demarcation of latitudinal wind anomalies for the EP El Niño shifts eastward, aligning around 160° E during the decaying spring. This shift reflects a dynamic atmospheric response to the evolving SSTA (Figure 7c). Conversely, the boundary for the CP El Niño shows minimal eastward adjustment, indicating a more stable atmospheric response despite the seasonal changes

(Figure 7d). The negative SSTA in the NWP thus produces characteristics similar to the differences in the circulation response, with the EP negative SSTA during the DJF period confined to the east of the Philippine Islands, while the CP negative SSTA can extend westward (Figure 7a,b). There are clear differences in the overall strength and coverage of the negative SSTA between the two types. The differences in the characteristics of the EP negative SSTA during the decaying spring are similar to those during the DJF period. However, the CP El Niño positive SSTA continues to expand westward around 160° longitude. Meanwhile, the NWP negative SSTA is weakened and cannot extend westward, which could be attributed to the weaker strength of the CP El Niño-related anomalous features (Figure 7c,d). The NWPAAC, as a critical component of the anomalous circulation response, produces corresponding differences in the context of the significant differences between the two types of El Niño cases.

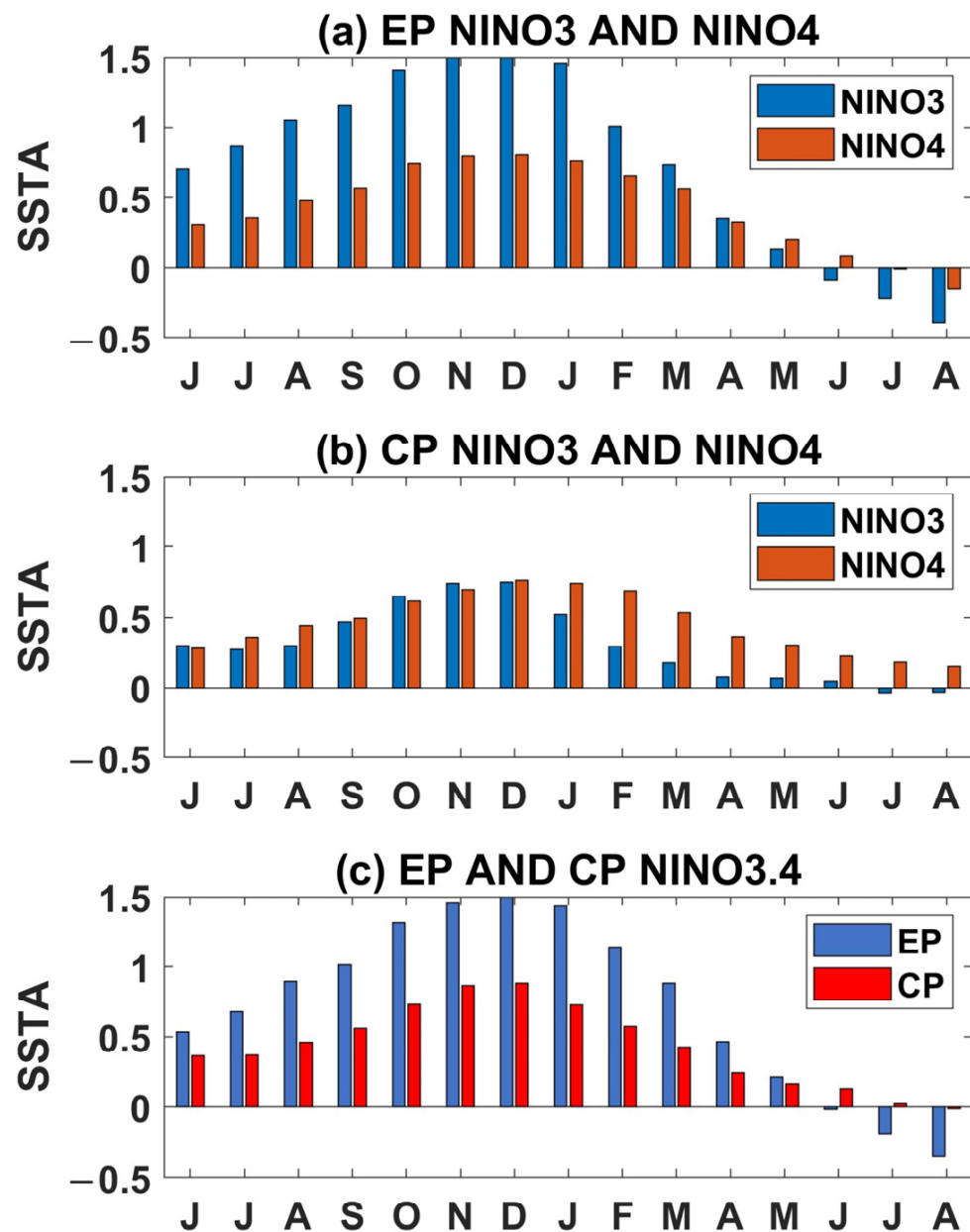


Figure 6. Composite of monthly SSTAs (unit: °C) averaged over the Niño 3 (5° S–5° N, 150° W–90° W) and Niño 4 (5° S–5° N, 160° E–150° W) for the (a) EP El Niño and (b) CP El Niño cases. (c) Composite of monthly SSTAs (unit: °C) averaged over the Niño 3.4 (5° S–5° N, 170° W–120° W) for the EP El Niño and CP El Niño cases.

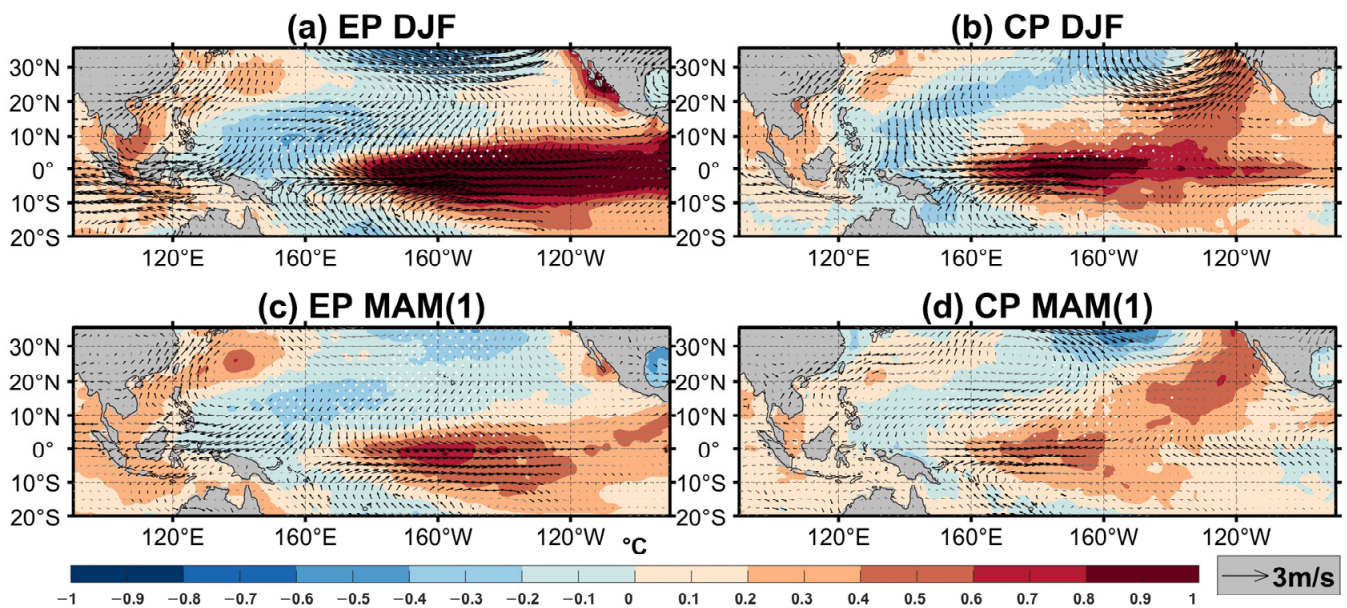


Figure 7. Composites of DJF SSTA (unit: °C) and 850 hPa wind anomalies (unit: m/s) in the (a) EP El Niño and (b) CP El Niño cases. Composites of MAM SSTA and 850 hPa wind anomalies in the (c) EP El Niño and (d) CP El Niño cases. The dotted areas and black arrowheads indicate the composite anomalies above the 95% confidence level.

As an essential bridge between El Niño and the East Asian circulation, changes in the NWPAAC can directly affect the East Asian circulation [12,17,21,34]. This study delineates the differences in the NWPAAC responses induced by El Niño, which are primarily attributed to the distinct SSTA characteristics and their respective impacts on the NWP region [17]. The locations of anomalous anticyclones induced by the EP and CP El Niño from winter to the following year's spring are different, and the seasonal differences are apparent. During the DJF period, the central locations of the EP-induced anomalous anticyclones are situated east of the Philippine Islands, whereas the CP-induced central locations are slightly westward over the Philippine Islands (Figure 7a,b). These differences become more pronounced in the spring, with the EP central locations not only shifting eastward in longitude but also northward in latitude, compared to its DJF characteristics. Conversely, the CP El Niño central locations show a westward shift, though the change in central location from winter to the decaying spring is less marked (Figure 7c,d). This seasonal variation reflects that the difference between the center locations of the two types of El Niño-induced NWPAAC gradually become significant as El Niño decays.

In addition to the differences in location, there are also significant differences in the NWPAAC intensity. Consistent with the characteristics of the SSTAs and circulation anomalies mentioned above, the NWPAAC associated with the EP El Niño is more robust and has a more significant impact area than the CP El Niño, especially the wind anomalies in Southeast Asia and the equatorial region. The strengthening wind affects the anomalous flow in SC, with a significant anomalous southwesterly flow in the region during the mature stage (DJF) of both the El Niño cases. However, the EP El Niño exhibits higher wind speeds and a broader area of the anomalous wind field, extending towards southern Japan and north of the Yangtze–Huaihe valley. In contrast, the CP El Niño generally presents weaker wind anomalies and barely affects these regions directly (Figure 7).

The NWPAAC exhibits significant seasonal variations, influencing the East Asian circulation by altering anomalous wind flows [3–6]. Initially, during the DJF period, both types of El Niño induce similar anomalous southwesterly winds (Figure 7c). However, these wind patterns diverge markedly (Figure 7d), with notable changes in wind direction, strength, and influence area, particularly in SC and the Yangtze–Huaihe valley. This

variability plays a key role in the differing responses of regional circulation to each El Niño type in East Asia.

Figure 8 shows a composite of the two types of El Niño 850 hPa stream function anomalies at springtime, with the location–intensity relationship of the NWPAAC much more straightforward and more pronounced. The center of the EP El Niño-related NWPAAC is located near 135° E, extending across the entire Philippine Sea, while the CP El Niño-related NWPAAC is centered roughly around 120° E, with a smaller coverage of influence than the EP El Niño (Figure 8). The longitudinal differences in the NWPAAC central locations are more pronounced than the latitudinal ones, with the CP El Niño located slightly southward compared to the EP El Niño. Additionally, anomalies in the water vapor flux during the decaying spring further corroborate the differences between the two types of NWPAAC: the EP El Niño is connected with strong water vapor dispersion west of the Philippine Islands, whereas the CP El Niño displays only limited water vapor dispersion around the Philippine Islands (Figure 9). Both the stream function analysis and the water vapor flux divergence demonstrate that the intensity and central location of the NWPAAC are tightly linked to the different El Niño cases.

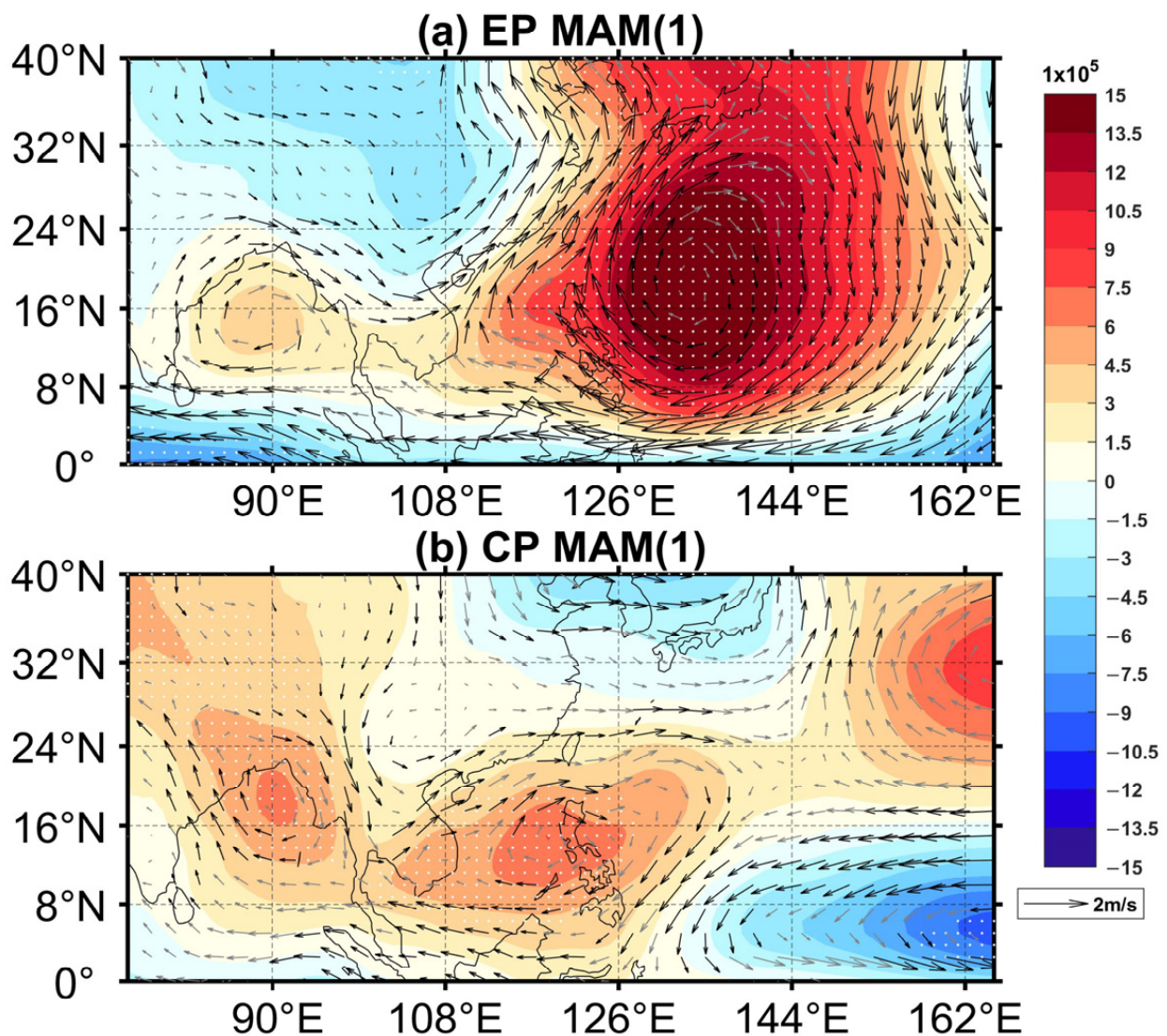


Figure 8. Composites of MAM 850 hPa stream function (unit: m^2/s) anomalies and 850 hPa rotating wind anomalies (unit: m/s) in the (a) EP El Niño and (b) CP El Niño cases. The dotted area and black arrowhead indicate the composite anomalies above the 95% confidence level.

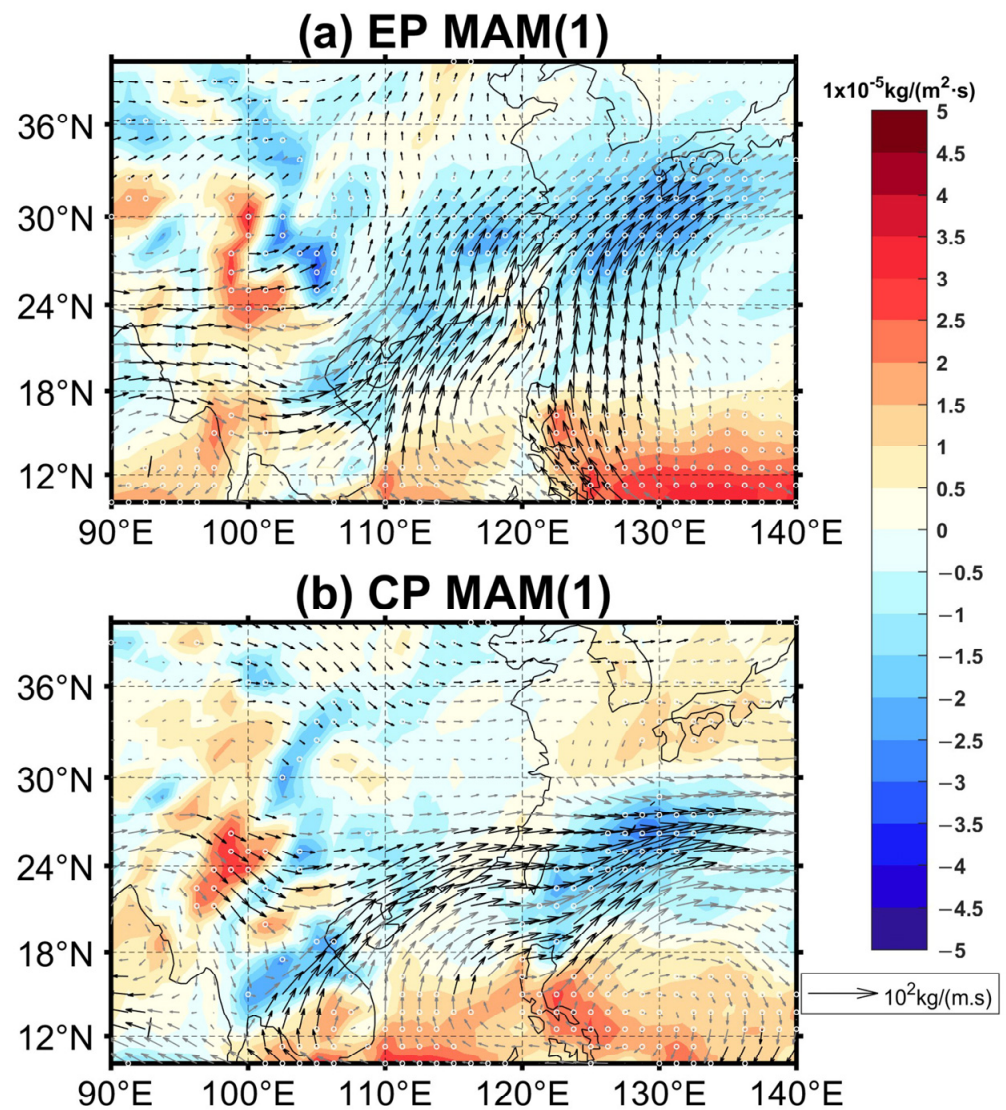


Figure 9. Composites of MAM water vapor flux divergence anomalies (unit: 10^{-5} kg/($m^2 \cdot s$)) and water vapor flux anomalies (unit: 10^2 kg/($m \cdot s$)) in the (a) EP El Niño and (b) CP El Niño cases. The dotted area and black arrowhead indicate the composite anomalies above the 95% confidence level.

How do the different NWPAAC responses have different impacts on the East Asian circulation? There are many well-established theories and research results on the EP El Niño [2,5,7]. In summary, the NWPAAC induced by the EP El Niño in spring is located west of the Philippine Islands. SC lies to the northwest of this anticyclone. The anomalous southwesterly flow covers most of SC and brings a large amount of warm and humid moisture from the tropics, creating favorable conditions for precipitation in the Yangtze–Huaihe valley (Figures 5a, 7a and 8a). The strong anomalous southwesterly flow even continues along the coast of China and penetrates deeper into northern China (Figure 8a), transporting air moisture to areas farther north.

During the spring following the CP El Niño, the atmospheric response in eastern China is different from that of the EP El Niño due to the significant difference in the location and intensity of the NWPAAC from that of the EP El Niño. In short, the central location of the NWPAAC in the CP El Niño decaying spring is more westward, with less intensity and influence, which implies that the NWPAAC associated with the CP El Niño has less impact on eastern China (Figure 8). During the CP El Niño cases, the anomalous flow is weaker and confined south of 26° N compared to the anomalous southwesterly flow during the EP El Niño cases, and the features of water vapor transport are also similar to

those of an abnormal low-level wind field (Figures 8b and 9b). Due to the weakening of intensity and the shift in the central position, the NWPAAC induced by the CP El Niño is located westward, with SC on its northward side. This causes the anomalous southwesterly winds on the northwest side of the CP El Niño to be gradually deflected clockwise after passing through the Beibu Gulf and to transform into anomalous westerly winds at the mouth of the Pearl River (Figure 8b). There are no significant anomalous flows north of 26° N in China. These wind anomalies may affect water vapor transport differently. The CP El Niño-induced water vapor transport anomalies are similar to the 850 hPa wind field anomalies, and abnormal water vapor transport is limited to south of 26° N (Figure 9b). Additionally, the shifting direction of the anomalous flow makes northerly water vapor transport more difficult: the deflection of the 850 hPa wind field will force the meridional component of the water vapor transport to gradually become latitudinal. To sum up, the spring water vapor flux anomaly under the EP El Niño case can even extend from SC to the Korean Peninsula and southern Japan, while it is confined to south of 30° N for the CP El Niño case.

5. Summary and Discussion

This study shows the different precipitation responses over eastern China in the decaying springs of the two types of El Niño, i.e., the EP and CP El Niño cases. Figure 10 illustrates the inter-seasonal relationships of the winter NCT and NWP indices with the spring precipitation in eastern China during our study period. The NCT index bears a relatively larger correlation with the anomalous spring precipitation in eastern China (Figure 10a), while the NWP index is barely correlated with the precipitation anomaly (Figure 10b). This implies that the EP El Niño SSTA–precipitation relationship is stronger than the CP El Niño SSTA–precipitation relationship. In other words, the warm winter SSTA over the tropical eastern Pacific is more likely to result in a following spring precipitation anomaly in eastern China. In particular, the EP El Niño results in excessive spring precipitation in eastern China, particularly in the Yangtze–Huaihe valley, whereas the CP El Niño leads to few changes in the eastern China precipitation.

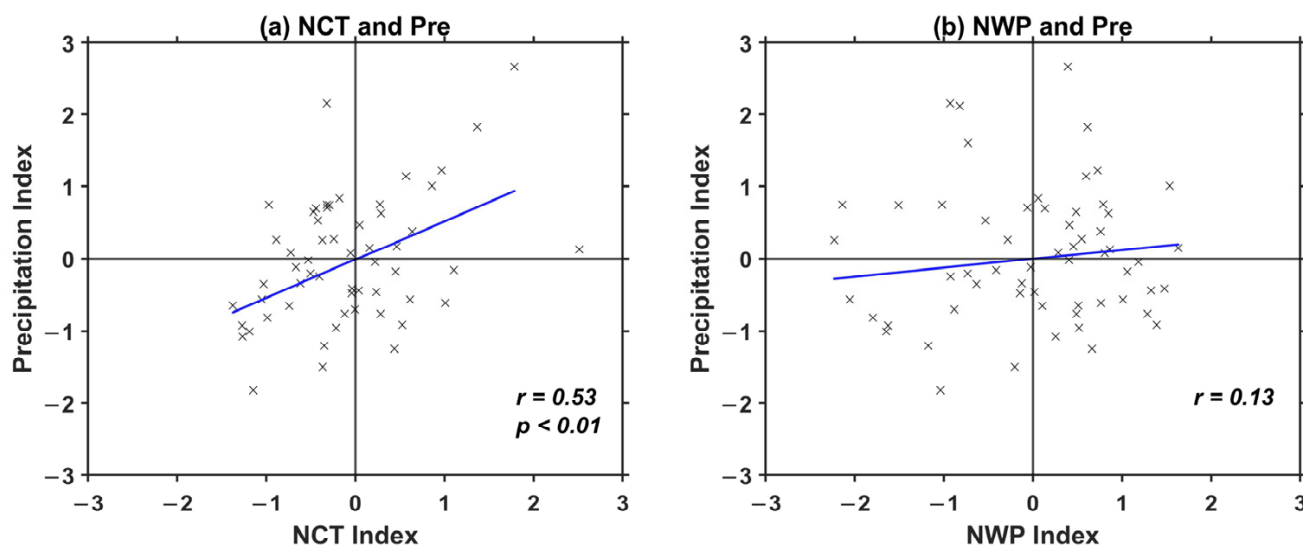


Figure 10. Scatterplots (a) between the normalized SSTA [spring precipitation averaged over eastern China (20° S–40° N, 110° E–125° E)] and winter NCT indices, and (b) the normalized SSTA and winter NWP indices during 1961–2020. The term r denotes the corresponding correlation coefficient for each panel. All data are linearly detrended and standardized for the correlation analysis.

The changes in precipitation responses are primarily driven by the different El Niño-related SSTA patterns in the tropical central–eastern Pacific. The NWPAAC plays a crucial role in the El Niño–precipitation relationship. As shown in Figure 11, the central longitude

and influencing range of the spring NWPAAC vary with the El Niño cases. For the EP El Niño cases, the warm SSTA centers are located more eastward and are relatively stronger. Thus, the El Niño-induced NWPAAC is mainly sited over the east of the Philippines with a relatively larger coverage. This influences the water vapor transport and subsequently leads to spring precipitation anomalies in SC, the Yangtze–Huaihe valley, and even southern Japan. For the CP El Niño decaying spring, the NWPAAC shifted westward with significantly reduced intensity and influencing range due to the westward shift and weaker intensity of the SSTA center compared to the EP El Niño. Under such circumstances, the SC is barely affected by the anomalous atmospheric circulation, exhibiting no evident local precipitation anomalies.

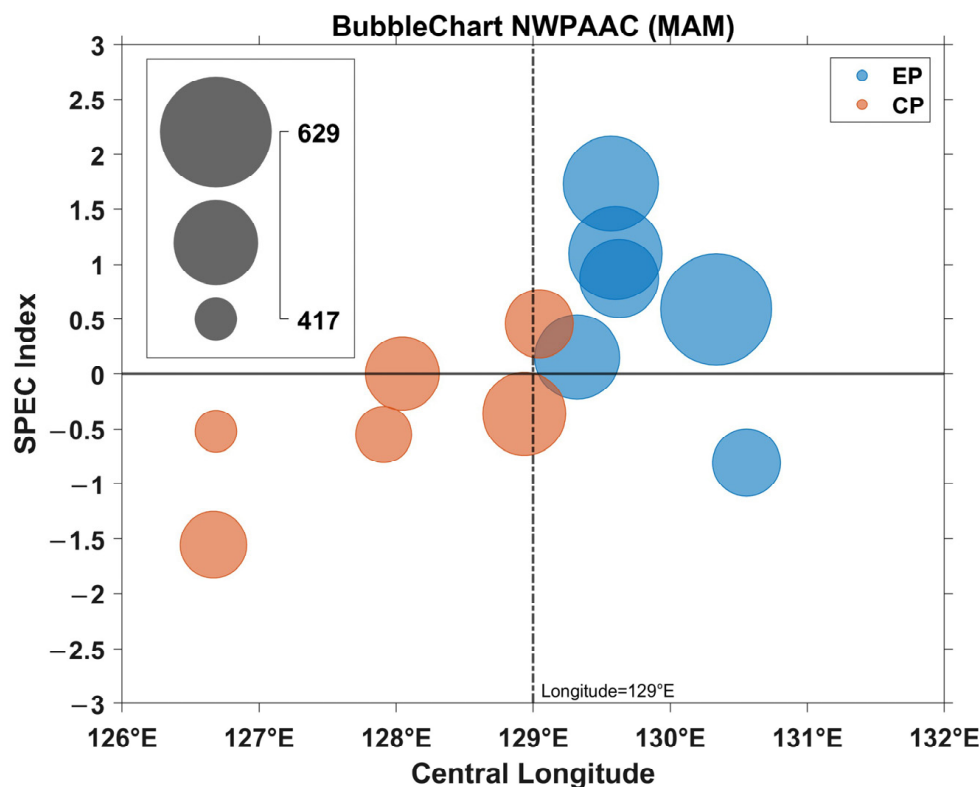


Figure 11. Bubble chart representing the relationship between the central longitude of significant vorticity anomalies and the normalized SPEC index (Figure 10) for 12 El Niño events (the first six EP El Niño cases are selected according to the spring Niño 3.4 index, the same as the CP El Niño) during the decaying spring within the region 5° N–40° N and 105° E–150° E. The size of each bubble corresponds to the number of grid points that indicate anomalies above the 95% confidence level, with larger bubbles indicating more significant grid points. The x -axis denotes the average central longitude of significant vorticity anomalies (exceeding the 95% confidence level), while the y -axis indicates the normalized SPEC index.

Recent research and observations indicate an obvious increase in the frequency of the CP El Niño cases since the 1990s, with projections suggesting a continued rise in their occurrence under the influence of global warming [8,35]. Moreover, studies have demonstrated that the amplitude of the EP El Niño cases is also expected to intensify in a warming climate, accompanied by an increase in the frequency of associated climate anomalies and extreme weather events [36,37]. This trend suggests that the differences between the SSTA patterns and the resulting climate responses in these two types of El Niño events will tend to be more pronounced and extreme in the future. Therefore, understanding the distinct impacts of the CP and EP El Niño events on climate states in eastern China is crucial for improving climate prediction and enhancing future disaster prevention and mitigation capabilities.

Author Contributions: D.Z. and C.G. designed and organized this research. Z.Y. (Zhichao Yang), Z.Y. (Zhi Yuan), X.W., B.X. and H.Q. analyzed the data. D.Z. and C.G. wrote the manuscript. All authors have read and agreed to the published version of the manuscript.

Funding: This work is supported by the National Natural Science Foundation of China (grant no. 42105025) and the China Postdoctoral Science Foundation (grant no. 2021M690862).

Institutional Review Board Statement: Not applicable.

Informed Consent Statement: Not applicable.

Data Availability Statement: The CRU precipitation data were obtained from <https://crudata.uea.ac.uk/cru/data/hrg> (accessed on 18 May 2024). The Hadley SST data were obtained from <https://www.metoffice.gov.uk/hadobs/hadisst/data/download.html> (accessed on 18 May 2024). The JRA55 atmospheric reanalysis data are available at https://jra.kishou.go.jp/JRA-55/index_en.html (accessed on 18 May 2024). The Monthly SST index from the National Oceanic and Atmospheric Administration (NOAA) Monthly SST index (ERSSTv5) is available at <https://www.cpc.ncep.noaa.gov/data/indices/> (accessed on 18 May 2024).

Conflicts of Interest: The authors declare no conflicts of interest.

References

1. Yuan, Y.; Yang, S. Impacts of different types of El Niño on the east Asian climate: Focus on Enso cycles. *J. Clim.* **2012**, *25*, 7702–7722. [[CrossRef](#)]
2. Wang, B.; Wu, R.; Fu, X. Pacific–east Asian teleconnection: How does Enso affect east Asian climate? *J. Clim.* **2000**, *13*, 1517–1536. [[CrossRef](#)]
3. Wang, B.; Zhang, Q. Pacific–east Asian teleconnection. Part ii: How the Philippine sea anomalous anticyclone is established during El Niño development. *J. Clim.* **2002**, *15*, 3252–3265. [[CrossRef](#)]
4. Wu, R.; Hu, Z.-Z.; Kirtman, B.P. Evolution of Enso-related rainfall anomalies in east Asia. *J. Clim.* **2003**, *16*, 3742–3758. [[CrossRef](#)]
5. Sampe, T.; Huang, G.; Du, Y.; Tokinaga, H.; Hafner, J.; Hu, K.; Xie, S.-P. Indian ocean capacitor effect on Indo–western pacific climate during the summer following El Niño. *J. Clim.* **2009**, *22*, 730–747. [[CrossRef](#)]
6. Jin, F.-F.; Stuecker, M.F.; Timmermann, A.; McGregor, S. Combination mode dynamics of the anomalous northwest pacific anticyclone. *J. Clim.* **2015**, *28*, 1093–1111. [[CrossRef](#)]
7. Feng, J.; Chen, W.; Tam, C.Y.; Zhou, W. Different impacts of El Niño and El Niño Modoki on China rainfall in the decaying phases. *Int. J. Climatol.* **2010**, *31*, 2091–2101. [[CrossRef](#)]
8. Lee, T.; McPhaden, M.J. Increasing intensity of El Niño in the central-equatorial pacific. *Geophys. Res. Lett.* **2010**, *37*, L14603. [[CrossRef](#)]
9. Ashok, K.; Behera, S.K.; Rao, S.A.; Weng, H.; Yamagata, T. El Niño Modoki and its possible teleconnection. *J. Geophys. Res.* **2007**, *112*, C11007. [[CrossRef](#)]
10. Jin, F.-F.; Kug, J.-S.; An, S.-I. Two types of El Niño events: Cold tongue El Niño and warm pool El Niño. *J. Clim.* **2009**, *22*, 1499–1515. [[CrossRef](#)]
11. Yu, J.Y.; Kim, S.T. Identifying the types of major El Niño events since 1870. *Int. J. Climatol.* **2012**, *33*, 2105–2112. [[CrossRef](#)]
12. Zhang, W.; Jin, F.-F.; Li, J.; Ren, H.-L. Contrasting impacts of two-type El Niño over the western north pacific during boreal autumn. *J. Meteorol. Soc. Jpn. Ser. II* **2011**, *89*, 563–569. [[CrossRef](#)]
13. Capotondi, A.; Wittenberg, A.T.; Newman, M.; Di Lorenzo, E.; Yu, J.-Y.; Braconnot, P.; Cole, J.; Dewitte, B.; Giese, B.; Guilyardi, E.; et al. Understanding Enso diversity. *Bull. Am. Meteorol. Soc.* **2015**, *96*, 921–938. [[CrossRef](#)]
14. Yu, J.-Y.; Kao, H.-Y. Contrasting eastern-pacific and central-pacific types of Enso. *J. Clim.* **2009**, *22*, 615–632. [[CrossRef](#)]
15. Smith, L.; Trenberth, K.E. Variations in the three-dimensional structure of the atmospheric circulation with different flavors of El Niño. *J. Clim.* **2009**, *22*, 2978–2991. [[CrossRef](#)]
16. Li, W.; Zhai, P. Relationship between Enso and frequency of extreme precipitation days in China. *Adv. Clim. Chang. Res.* **2009**, *5*, 336–342. [[CrossRef](#)]
17. Yu, T.; Feng, J.; Chen, W.; Wang, X. Persistence and breakdown of the western north pacific anomalous anticyclone during the ep and cp El Niño decaying spring. *Clim. Dyn.* **2021**, *57*, 3529–3544. [[CrossRef](#)]
18. Feng, J.; Li, J. Influence of El Niño Modoki on spring rainfall over south China. *J. Geophys. Res.* **2011**, *116*, D13102. [[CrossRef](#)]
19. Zeng, Z.; Sun, J. Influence of different configurations of western north pacific anticyclone and Siberian high on spring climate over China. *Int. J. Climatol.* **2023**, *43*, 2699–2718. [[CrossRef](#)]
20. Xue, X.; Chen, W.; Chen, S.; Zhou, D. Modulation of the connection between boreal winter Enso and the south Asian high in the following summer by the stratospheric quasi-biennial oscillation. *J. Geophys. Res. Atmos.* **2015**, *120*, 7393–7411. [[CrossRef](#)]
21. Zhang, R.; Min, Q.; Su, J. Impact of El Niño on atmospheric circulations over east Asia and rainfall in China: Role of the anomalous western north pacific anticyclone. *Sci. China Earth Sci.* **2017**, *60*, 1124–1132. [[CrossRef](#)]

22. Gao, C.; Li, G. Decadal enhancement in the effect of El Niño in the decaying stage on the pre-flood season precipitation over southern China. *J. Clim.* **2023**, *36*, 8155–8170. [[CrossRef](#)]
23. Rayner, N.A.; Parker, D.E.; Horton, E.B.; Folland, C.K.; Alexander, L.V.; Rowell, D.P.; Kent, E.C.; Kaplan, A. Global analyses of sea surface temperature, sea ice, and night marine air temperature since the late nineteenth century. *J. Geophys. Res. Atmos.* **2003**, *108*, 4407. [[CrossRef](#)]
24. Kobayashi, S.; Ota, Y.; Harada, Y.; Ebata, A.; Moriya, M.; Onoda, H.; Onogi, K.; Kamahori, H.; Kobayashi, C.; Endo, H.; et al. The JRA-55 reanalysis: General specifications and basic characteristics. *J. Meteorol. Soc. Jpn. Ser. II* **2015**, *93*, 5–48. [[CrossRef](#)]
25. Harris, I.; Osborn, T.J.; Jones, P.; Lister, D. Version 4 of the CRU TS monthly high-resolution gridded multivariate climate dataset. *Sci. Data* **2020**, *7*, 109. [[CrossRef](#)]
26. Ren, H.-L.; Jin, F.-F. Niño indices for two types of ENSO. *Geophys. Res. Lett.* **2011**, *38*, L04704. [[CrossRef](#)]
27. Freund, M.B.; Henley, B.J.; Karoly, D.J.; McGregor, H.V.; Abram, N.J.; Dommenget, D. Higher frequency of central Pacific El Niño events in recent decades relative to past centuries. *Nat. Geosci.* **2019**, *12*, 450–455. [[CrossRef](#)]
28. Zhang, C.; Li, T.; Li, S. Impacts of CP and EP El Niño events on the Antarctic sea ice in austral spring. *J. Clim.* **2021**, *34*, 9327–9348. [[CrossRef](#)]
29. Zhang, W.; Jiang, F.; Stuecker, M.F.; Jin, F.-F.; Timmermann, A. Spurious North Tropical Atlantic precursors to El Niño. *Nat. Commun.* **2021**, *12*, 3096. [[CrossRef](#)]
30. Xie, S.-P.; Kosaka, Y.; Du, Y.; Hu, K.; Chowdary, J.S.; Huang, G. Indo-western Pacific ocean capacitor and coherent climate anomalies in post-ENSO summer: A review. *Adv. Atmos. Sci.* **2016**, *33*, 411–432. [[CrossRef](#)]
31. Geng, X.; Zhang, W.; Jiang, F.; Stuecker, M.F.; Liu, C. Impacts of central Pacific El Niño on southern China spring precipitation controlled by its longitudinal position. *J. Clim.* **2019**, *32*, 7823–7836. [[CrossRef](#)]
32. Xu, K.; Zhu, C.; He, J. Two types of El Niño-related southern oscillation and their different impacts on global land precipitation. *Adv. Atmos. Sci.* **2013**, *30*, 1743–1757. [[CrossRef](#)]
33. Zhang, M.; Sun, J. Enhancement of the spring East China precipitation response to tropical sea surface temperature variability. *Clim. Dyn.* **2017**, *51*, 3009–3021. [[CrossRef](#)]
34. Zeng, Z.; Sun, J. Interannual variations in the intraseasonal variability of spring precipitation over southern China and the possible mechanisms. *J. Clim.* **2023**, *36*, 5319–5336. [[CrossRef](#)]
35. Feng, Y.; Chen, X.; Tung, K.-K. ENSO diversity and the recent appearance of central Pacific ENSO. *Clim. Dyn.* **2019**, *54*, 413–433. [[CrossRef](#)]
36. Geng, T.; Cai, W.; Wu, L.; Santoso, A.; Wang, G.; Jing, Z.; Gan, B.; Yang, Y.; Li, S.; Wang, S.; et al. Emergence of changing central-Pacific and eastern-Pacific El Niño-southern oscillation in a warming climate. *Nat. Commun.* **2022**, *13*, 6616. [[CrossRef](#)]
37. Shin, N.-Y.; Kug, J.-S.; Stuecker, M.F.; Jin, F.-F.; Timmermann, A.; Kim, G.-I. More frequent central Pacific El Niño and stronger eastern Pacific El Niño in a warmer climate. *Npj Clim. Atmos. Sci.* **2022**, *5*, 101. [[CrossRef](#)]

Disclaimer/Publisher’s Note: The statements, opinions and data contained in all publications are solely those of the individual author(s) and contributor(s) and not of MDPI and/or the editor(s). MDPI and/or the editor(s) disclaim responsibility for any injury to people or property resulting from any ideas, methods, instructions or products referred to in the content.